Phase-referenced probe interferometer for biological surface profiling and displacement measurements

Christopher Fang-Yen and Mark C. Chu
G. R. Harrison Spectroscopy Laboratory, Massachusetts Institute of Technology, Cambridge, Massachusetts 02139, USA

H. Sebastian Seung
Howard Hughes Medical Institute and Department of Brain and Cognitive Sciences, Massachusetts Institute of Technology, Cambridge, Massachusetts 02139, USA

Ramachandra R. Dasari and Michael S. Feld
G. R. Harrison Spectroscopy Laboratory, Massachusetts Institute of Technology, Cambridge, Massachusetts 02139, USA

(Received 1 September 2007; accepted 20 November 2007; published online 26 December 2007)

We present a probe-based, phase-referenced low coherence interferometer in which the reference field is provided by a fiber end reflection. A gradient-index microlens focuses light onto a sample and collects reflected light. We use the probe interferometer to measure surface profiles of the compound eye of a housefly (*Musca domestica*) and measure nanometer-scale vibrations in a test sample. © *2007 American Institute of Physics.* [DOI: 10.1063/1.2823976]

I. INTRODUCTION

In a number of low coherence interferometry schemes[1–4] the phase of light scattered from a sample is measured relative to a reflection from a nearby, intervening reference surface on the same optical path. This nearly common-path configuration, referred to here as phase-referenced interferometry, can be used to strongly reduce phase noise due to external perturbations.

Phase-referenced interferometry has proven to be particularly suitable for applications in biology. Studies based on two-wavelength interferometry[1] and spectral domain interferometry[2] have been used to measure motions in cultured cells; in these experiments the reference beam was provided by reflection from the bottom of the coverslip on which the cells were attached. In phase-referenced dual-beam[3] and polarization-dependent[4] low coherence interferometers, reference surfaces were positioned above the samples to measure nanometer-scale surface displacements in nerves during the action potential.[5]

Two aspects of phase-referenced interferometry may be problematic in some situations. First, it requires a reference surface to be in reasonably close proximity to the sample of interest and aligned to reflect the incident beam back to the interferometer optics. In many situations such a configuration may be difficult or inconvenient to achieve. Space for the reference surface may be limited, and the reference surface may impede access to the sample. The reference surface may need to be adjusted in position and/or angle if more than one point on the sample is to be investigated, or if the sample changes position or orientation significantly during the experiment. Therefore, it would be desirable to have a system in which no separate reference surface is required.

A second difficulty is a limitation in numerical aperture (NA) of the light delivery and collection optics due to the axial separation between sample and reference. High NA may be desirable to obtain very small transverse focus size and for optical sectioning in three-dimensional samples by confocal imaging. For a high-NA beam with approximately spherical wavefront converging onto the sample, reflections from sample and reference have apparent source locations separated by roughly twice the distance between sample and reference surface. For sample and reference surfaces to be simultaneously in focus, their separation must be on the order of the depth of field $\sim\lambda/\mathrm{NA}^2$ or smaller. This requirement is clearly difficult to meet for $\mathrm{NA}\sim 1$. (We have assumed the reference surface is flat; a spherical concave reference surface could create a reflected field matching the sample wavefront, but would be difficult to align and would restrict the beam to a single position.) Although the simultaneous focus of sample and reference is not strictly required for interferometry, a low reference reflection collection efficiency will degrade signal-to-noise ratio and/or imaging speed for a given probe beam power.

II. METHODS

We have designed a phase-referenced interferometer in which the reference field is created by a Fresnel reflection from a cleaved fiber tip located inside a small optical fiber probe. Light transmitted by the fiber is focused onto the sample through a gradient-index (GRIN) microlens. Since the reference reflection is included within the probe, a separate reference surface is no longer required. Furthermore, the NA of the system is limited only by the NA of the focusing lens, allowing a transverse spot size at focus comparable to the wavelength of light used.

Interferometric fiber optic probes are used with biological tissues in laser Doppler vibrometry[6,7] and optical coherence tomography (OCT).[8,9] A probe-based laser interferometer has been described for vibration measurements in biological systems.[10] Another interferometer has used a three fiber geometry to reduce the effects of external

 © 2007 American Institute of Physics

Author complimentary copy. Redistribution subject to AIP license or copyright, see http://rsi.aip.org/rsi/copyright.jsp

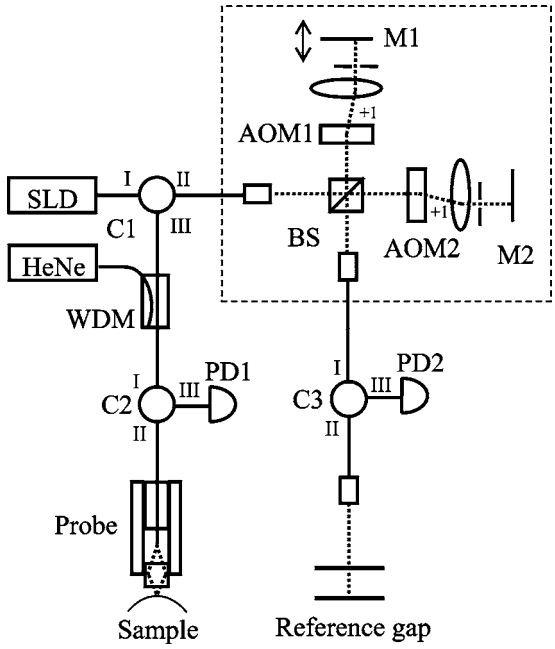

FIG. 1. Phase-referenced probe interferometer setup. Dashed box indicates Michelson interferometer. SLD: superluminescent diode; AOM1, AOM2: acousto-optic modulators, M1, M2: mirrors; C1–C3: optical circulators; BS: beam splitter; PD1, PD2: photodetectors, HeNe: helium-neon guide laser, WDM: wavelength division multiplexer.

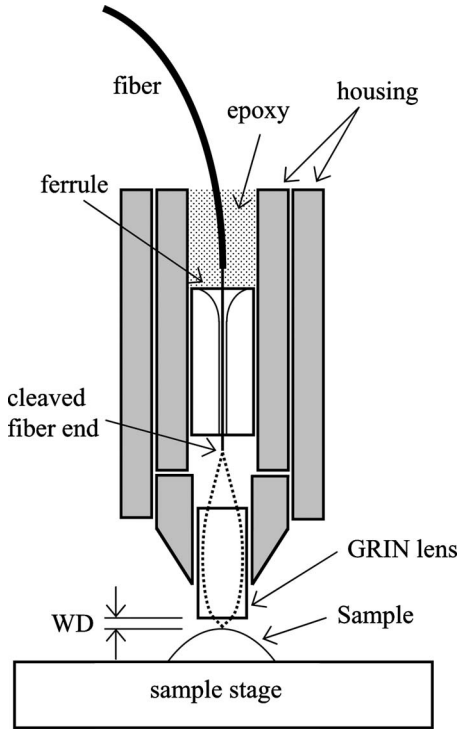

FIG. 2. Detail of probe assembly. WD: working distance, approximately 0.5 mm.

disturbances.[11] However, to our knowledge, there have been no reports of phase-referenced probes in a low coherence interferometer.

Our interferometer (Fig. 1) resembles the design presented in Ref. 3. Broadband light from a superluminescent diode [Superlum SLD-761, center wavelength of 1549 nm, full width at half maximum (FWHM) bandwidth of 49 nm] enters a Michelson interferometer containing acousto-optic modulators driven at frequencies $\omega_1 = 110.05$ MHz and $\omega_2 = 110$ MHz, each aligned in a double-pass configuration. The outputs from the two ports of the interferometer are routed via optical circulators to the probe (Fig. 2) and a reference gap composed of two glass windows separated by an adjustable distance. Reflected light from these elements are detected by two ac-coupled photodetectors. A 632.8 nm helium-neon laser (Melles Griot), coupled to the beam through a wavelength-division multiplexer (Koncent Photonics) helps to visualize the probe output for alignment.

Optics are adjusted so that the following optical path delays are equal to well within the coherence length: (i) ΔL, between the two Michelson interferometer arms; (ii) ΔL_S, between the sample reflection and probe fiber reflection; and (iii) ΔL_R, between the two reflections from the reference gap. The photodetectors then record heterodyne signals at frequency $\Omega = 2(\omega_1 - \omega_2) = 100$ kHz. The photodetector outputs are digitized by a 12 bit analog-to-digital converter card (National Instruments PCI-6110) and a computer calculates the phase difference $\Delta\phi(t)$ between the two signals. The phase difference $\Delta\phi(t) = k_0(\Delta L_S - \Delta L_R)$, where k_0 is the peak wave number of the source, represents the phase of the sample reflection relative to the probe reference reflection, assuming a time-independent reference gap. The phase shift can then be expressed as a displacement $\Delta d(t) = \Delta\phi(t)/2k_0$.

The probe (Fig. 2) was constructed as follows. A single mode optical fiber was stripped and cleaved at a right angle using a fiber cleaver so that a backreflection of about 3% was achieved. The cleaved fiber end was inserted into a 2.8 mm diameter glass ferrule. Cylindrical aluminum housings positioned the ferrule and a 0.29-pitch GRIN lens (Newport LGI1560, 0.46 NA) as shown. The GRIN lens is antireflection coated for the wavelengths used. The distance between the fiber tip and interior face of the GRIN lens is approximately 4 mm; the working distance (WD) between the tip of the GRIN lens and the focus is 0.5 mm. The focus spot diameter is estimated to be ≈ 2 μm FWHM.

To test the probe stability, we mounted the probe in a cage plate assembly (Thorlabs) with a fixed glass surface positioned at the sample focus. With a probe output power of 200 μW, the total noise between 1 Hz and 1 kHz was approximately 0.2 mrad (rms), corresponding to a displacement of 0.02 nm.

III. RESULTS

For the imaging experiments, samples were raster scanned under the fixed probe by a *XY* translation stage with motorized actuators. We first imaged the spherical surface of a plano-convex lens (focal length of 75 mm) to confirm the accuracy of the phase measurements. A 400 μm long cross section of the phase map through the center of the lens was phase unwrapped to remove 2π ambiguity. The measured radius of curvature (ROC) of 37.1 ± 1.5 mm determined by a quadratic fit to the resulting height profile was in agreement with the lens manufacturer specified ROC of 38.6 ± 0.5 mm.

To demonstrate the biological imaging capabilities of the probe, we used the probe to image a small region from the

Author complimentary copy. Redistribution subject to AIP license or copyright, see http://rsi.aip.org/rsi/copyright.jsp

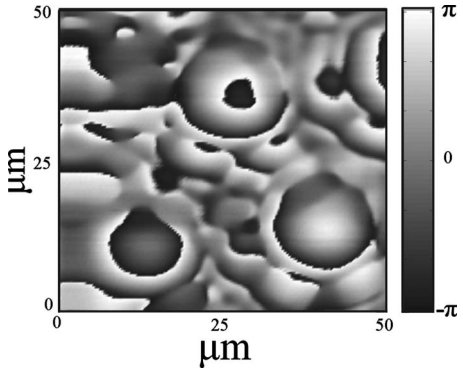

FIG. 3. Phase image from compound eye of a fly, showing three facets. Pixel size of 0.5 μm.

compound eye of a housefly (*Musca domestica*). The outer surface of the compound eye is composed of a hexagonal lattice of facets, which are front lens surfaces of the ommatidia, cone-shaped structures for light collection and detection. For our images, a portion of the fly's compound eye was dissected and mounted on the translation stage to present a surface approximately perpendicular to the probe beam. The probe position was adjusted to maximize the reflected power at the center of facets (peak reflectivity $\approx 10\%$).

Figure 3 shows a scanned-sample phase map of a 50×50 μm^2 region. Ring patterns corresponding to three circular facets are visible. A cross section of a single facet was phase unwrapped to remove 2π ambiguity and converted to a distance. The resulting profile is shown in Fig. 4 with a best-fit second order polynomial. The curvature at the center of the parabola corresponds to a ROC of 36.8 μm. Measurements of ommatidium facet curvature have previously been performed via electron microscopy, with resulting ROC values ranging from 13.6 to 28.0 μm for the dung beetle compound eye.[12]

To demonstrate the probe interferometer's ability to measure small, rapid motions, we first measured driven vibrations of a reflective surface. A small piece of microscope slide glass was glued to a multilayer piezomodulator and its front surface aligned to back reflect the focused probe beam. The piezomodulator was driven by a sine wave using a digital function generator. Figure 5 shows time-dependent displacement for oscillation of 0.9 nm peak-peak amplitude and drive frequency of 150.0 Hz. Calculation of the peak frequency f_0 of the power spectrum from a 10 s long displacement gave $f_0 = 150.0 \pm 0.1$ Hz.

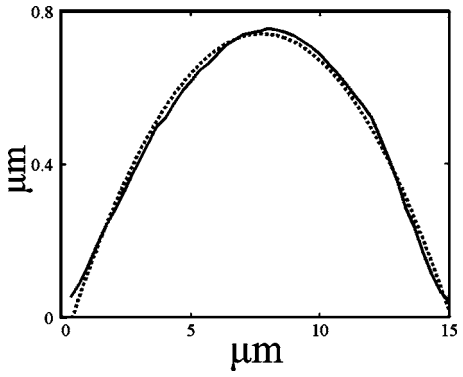

FIG. 4. Solid line: cross section of single fly eye facet (lower left in Fig. 3). Dashed line: fit to $y=ax^2+bx+c$, with $a=-0.0138$ μm^{-1}, $b=0.2135$, and $c=-0.0929$ μm.

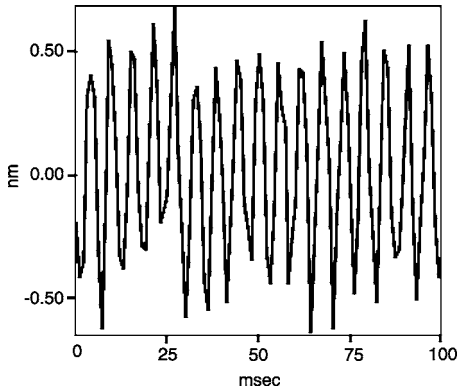

FIG. 5. 0.9 nm, 150 Hz oscillations of a piezodriven glass surface measured by probe interferometer.

We have also used the probe interferometer to measure nanometer-scale surface displacements in a lobster nerve during the action potential (data not shown). The amplitude and duration of displacements measured during the action potential were comparable to those observed earlier.[3]

IV. CONCLUSIONS

We have developed a probe-based interferometer which addresses problems associated with the conventional phase-referenced geometry, and demonstrated its abilities for high resolution imaging and displacement measurements. The small spot size of the probe beam will allow its use in the measurement of cell membrane displacements in single cells. The probe may also find applications as an all-optical sensor[13] for motions, vibration, or sound.

ACKNOWLEDGMENTS

This work was supported by the National Institutes of Health (P41-RR02594-18) and Hamamatsu Corporation.

[1] C. Yang, A. Wax, M. S. Hahn, K. Badizadegan, R. R. Dasari, and M. S. Feld, Opt. Lett. **26**, 1271 (2001).
[2] M. A. Choma, A. K. Ellerbee, C. H. Yang, T. L. Creazzo, and J. A. Izatt, Opt. Lett. **30**, 1162 (2005).
[3] C. Fang-Yen, M. C. Chu, H. S. Seung, R. R. Dasari, and M. S. Feld, Opt. Lett. **29**, 2028 (2004).
[4] T. Akkin, D. P. Dave, T. E. Milner, and H. G. Rylander, Opt. Express **12**, 2377 (2004).
[5] I. Tasaki, Physiol. Chem. Phys. Med. NMR **20**, 251 (1988).
[6] L. E. Drain, *The Laser Doppler Technique* (Wiley, New York, 1980).
[7] R. L. Goode, G. Ball, S. Nishihara, and K. Nakamura, Am. J. Otol. **17**, 813 (1996).
[8] D. Huang, E. A. Swanson, C. P. Lin, J. S. Schuman, W. G. Stinson, W. Chang, M. R. Hee, T. Flotte, K. Gregory, C. A. Puliafito, and J. G. Fujimoto, Science **254**, 1178 (1991).
[9] A. M. Rollins, R. Ung-arunyawee, A. Chak, R. C. K. Wong, K. Kobayashi, M. V. Sivak, and J. A. Izatt, Opt. Lett. **24**, 1358 (1999).
[10] M. A. Nokes, B. C. Hill, and A. E. Barelli, Rev. Sci. Instrum. **49**, 722 (1978).
[11] N. Nakatani, T. Izumi, S. Asano, T. Yamada, and T. Sakabe, Rev. Sci. Instrum. **58**, 2161 (1987).
[12] N. Gokan and V. B. Meyer-Rochow, New Zealand Entomol. **58**, 7 (1990).
[13] B. Lee, Opt. Fiber Technol. **9**, 57 (2003).

Author complimentary copy. Redistribution subject to AIP license or copyright, see http://rsi.aip.org/rsi/copyright.jsp